Polymer Chemistry

PAPER

View Article Online
View Journal | View Issue

Cite this: *Polym. Chem.*, 2019, **10**, 5543

Role of pendant side-chain length in determining polymer 3D printability†

Tanmay Jain,[a] William Clay,[a,b] Yen-Ming Tseng,[a] Apoorva Vishwakarma,[a] Amal Narayanan,[a] Deliris Ortiz,[a] Qianhui Liu[a] and Abraham Joy *[a]

Received 16th June 2019,
Accepted 25th September 2019

DOI: 10.1039/c9py00879a

rsc.li/polymers

Three-dimensional (3D) printing allows for creation of patient-specific implants. However, development of new synthetic materials for 3D printing has been relatively slow with only a few polymers available for tissue engineering applications. Most of these polymers require harsh processing conditions like high temperatures and pressures or are mixed with a combination of leachable additives like plasticizers, initiators, crosslinkers, and solvents to enable 3D printing. Therefore, to propel the development of new polymers for ambient temperature, additive-free 3D printing it is necessary to systematically understand the relationship between the structure of a polymer with its 3D printability. Herein, three homopolyesters were synthesized, each with a common backbone but differing in the length of their saturated, aliphatic pendant chains with 2, 6, or 15 carbons. The physical properties such as the glass transition temperature (T_g) and the rheological properties like shear thinning, temperature response, and stress relaxation were correlated to the individual polymer's 3D printability. The 3D printability of the polymers was assessed based on four criteria: ability to be extruded as continuous filaments, shape fidelity, the retention of printed shape, and the ability to form free hanging filaments. We observed that the polymers with longer side chains can be extruded at low temperature and pressure because the long side chains act as internal diluents and increase the flowability of the polymer. However, their ability to retain the 3D printed shape is adversely affected by the increase in side chain length, unless the side chains form ordered structures leading to immediate recovery of viscosity. The insight derived from the systematic investigation of the effect of polymer structure on their rheology and 3D printability can be used to rationally design other polymers for extrusion-based direct-write 3D printing.

Introduction

The ability to efficiently fabricate customized constructs with intricate architectures makes 3D printing useful for a broad range of applications, including biomedical applications.[1–3] Personalized medical devices such as prosthetics, dentures, and implants are being regularly produced by 3D printing for hitherto unmet clinical needs.[3,4] The potential of 3D printing for creating customized implants has been demonstrated by successful clinical implantation of medical devices such as aortic valves, renal bladder, and tracheal splints.[1,5] However, the progress in developing 3D printing methodologies has significantly outpaced the design and availability of new 'biomaterial inks'.[6,7]

Extrusion-based direct-write 3D printing (EDP) is one of the most widespread techniques to fabricate devices and scaffolds for tissue engineering.[8] This is mainly because this technique is compatible with a wide range of materials and can produce 3D constructs with sizes and dimensions relevant to biomedical applications.[8,9] Inks with a wide viscosity range have been 3D printed using EDP.[1,8] In EDP, the material is extruded through a narrow nozzle and a 3D construct is formed layer-by-layer by depositing continuous filaments of the ink along a predetermined path. The 3D printed ink is permanently set by employing physical processes such as solvent evaporation, re-crystallization, or supramolecular interactions, or by chemical crosslinking through light or thermally controlled reactions.[1,8]

Currently, synthetic polymers like poly(lactic-*co*-glycolic acid) (PLGA), polycaprolactone (PCL), poly(methyl methacrylate) (PMMA), *etc*. are regularly used for EDP of medical devices.[8,10,11] Synthetic polymers such as the above are printed by either heating them to high temperatures or using processing aids like solvents, surfactants, or plasticizers.[12–14] In addition to the harsh processing conditions required to print

[a]*Department of Polymer Science, The University of Akron, 170 University Avenue, Akron, Ohio, 44325, USA. E-mail: abraham@uakron.edu*
[b]*Department of Chemistry & Biochemistry, The University of Mount Union, 1972 Clark Avenue, Alliance, OH, 44601, USA*

†Electronic supplementary information (ESI) available. See DOI: 10.1039/c9py00879a

these polymers, synthetic polymers used for EDP have limited independent tunability of processing, degradation, and mechanics.[8,12] Moreover, most of these polymers are not easy to functionalize with bioactive ligands and are therefore used mostly for space filling applications that allow basic cell function but do not actively promote biological activity.[7,11] On the other hand, hydrogels provide an attractive alternative that can be printed at mild conditions but lack the mechanical strength to create large constructs with high shape fidelity.[7] Moreover, most hydrogels are based on natural polymers like gelatin, chitosan, alginates, *etc*. that suffer from batch to batch inconsistencies and may provoke an immunogenic reaction.[9,16]

Therefore, a major challenge for the coming years will be to develop biodegradable polymer ink libraries with user-defined and tunable properties. Although some efforts are being made to design new polymer systems, these are still in their infancy. For example, our lab previously reported the synthesis and EDP of multifunctional polyesters at room temperature without the presence of solvents or external additives.[17–19] Other examples include supramolecular hydrogel inks that have been developed for extrusion-based 3D printing to create high resolution multi-material structures incorporated with live cells.[20] Other studies have described the extrusion based 3D printing of additive-free synthetic diblock and triblock polymers.[21–24] However, to the best of our knowledge, there are no studies that investigated the effect of systematically modifying polymer structure and studying its effect on polymer rheology and 3D printability.

To address the lack of structure-3D printability studies, we synthesized polyesters with a common backbone but differing in carbon chain length of pendant groups. The polyesters are formed using a previously reported method involving carbodiimide-mediated polyesterification of diols and diacids.[15,25] The polyesters are composed of equimolar ratio of succinic acid and *N*-substituted diols with varied saturated, aliphatic chain lengths of 2, 6, and 15 carbons. The polyesters are labelled $\mathbf{C_2}$, $\mathbf{C_6}$, and $\mathbf{C_{15}}$ respectively, where the subscript denotes the carbon chain length on the pendant group. The synthesized polyesters were characterized using ^{1}H nuclear magnetic resonance (NMR), gel permeation chromatography (GPC), differential scanning calorimetry (DSC), and shear rheology. Steady state flow tests were performed to determine the zero-shear viscosity and shear thinning ability of the synthesized polyesters. Small amplitude oscillatory shear (SAOS) measurements were performed to investigate the effect of polymer structure on the viscoelasticity of the polyesters. Stress relaxation experiments were performed to examine the transient properties of the polyesters. The polyesters were 3D printed using a pneumatic, extrusion-based direct-write technique and their 3D printability was evaluated. The printability of each polyester was assessed based on their ability to extrude as continuous filaments, the shape fidelity of the printed constructs, the ability to retain the printed shape, and the ability to form free hanging filaments. The printing temperature and pressure was adjusted to enable extrusion of continuous filaments. The shape fidelity was determined based on the shape of the pores of the 3D printed scaffolds with rectilinear infill pattern. The shape retention ability of the polymers was analyzed by monitoring the pore shape and area over time after printing. The polymer's ability to form a free hanging bridge was investigated by printing a continuous filament over pillars with predefined gaps between 0.5–16 mm. The insights derived from this study can be used to design a new class of polymers for extrusion-based direct-write 3D printing for tissue engineering applications.

Materials and methods

Materials

Chemical synthesis reagents include diethanolamine (>99.0%, TCI), ethyl propionate (99+%, Acros Organics), ethyl heptanoate (99%, Aldrich), methyl palmitate (97%, Alfa Aesar), sodium methoxide (98%, Alfa Aesar), succinic acid (Fisher Scientific), 4-(Dimethylamino)pyridinium 4-toluenesulfonate (DPTS, prepared according to literature[26]) and *N*,*N*′-Diisopropylcarbodiimide (DIC, 99.50%, Chem-Impex Int'l Inc.). Dichloromethane (Thermo Fischer Scientific) was dried *via* distillation over anhydrous CaH_2.

Instrumentation

^{1}H-NMR spectra of monomers and polymers were obtained in a 300 MHz Varian Mercury spectrophotometer in DMSO-d6 or $CDCl_3$, where chemical shifts (δ) were recorded in ppm relative to the solvent signal at 2.5 and 7.26 ppm, respectively. Glass transition temperature and the melting temperature were determined with a TA Instruments Q200 DSC. Each sample was sealed in hermetic aluminum pans and heated from −50 °C to 150 °C at a ramp rate of 10 °C min^{-1} under N_2 atmosphere. The heating and cooling processes were repeated 3 times. The number average molecular weight (M_n) and the weight average molecular weight (M_w) for each polyester were determined with a Tosoh HLC-8320GPC equipped with a RI detector with polystyrene as the standard and tetrahydrofuran as the eluent. Rheological properties of the polymers were determined using an ARES-G2 rotational rheometer using 8 mm parallel plates. The rheometer was equipped with a Force Convection Oven (FCO) for temperature control. The polymer was loaded on the rheometer plate as a melt and heated to a temperature of T_g +50 °C for 10 minutes to remove any residual stress before being equilibrated to the respective experiment's temperature for another 10 minutes. The shear rate sweep was performed in steady state mode. Before acquisition of each data point, the sample was allowed to equilibrate for 240 seconds. The temperature sweep was performed in the oscillatory mode whereas the stress relaxation step was performed in the transient mode. The %strain for the temperature sweeps and the stress relaxation steps was within the linear regime of each polymer as determined by performing a strain sweep.

Monomer synthesis procedure

The *N*-functionalized diethanolamide monomers (diols) were synthesized using similar procedures as reported by Gokhale

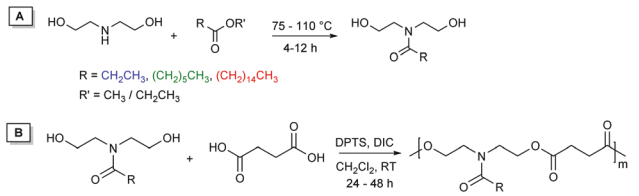

Scheme 1 General reaction scheme for the (A) monomers and (B) polyesters.

et al.[15] with minor modifications. Typically, a transmidation reaction between diethanolamine and a corresponding α-functionalized alkyl ester was performed to obtain the diethanolamide monomers with different pendant carbon lengths (Scheme 1A). The reaction mixtures were purified using column chromatography with silica as stationary phase and a mixture of 10% methanol and 90% dichloromethane as eluent. The purified compounds were characterized using ^{1}H NMR spectroscopy and the details of the synthesis and characterization of the individual monomers are given below.

Synthesis of *N*,*N*-bis(2-hydroxyethyl)propionamide (mC_2). In a round bottom flask with a magnetic stir bar, diethanolamine (6.30 g, 60.0 mmol) and ethyl propionate (3.06 g, 30.0 mmol) were refluxed at 80 °C for 4 h. The obtained product was a white solid after purification using column chromatography. **mC_2**: Yield = 82%, ^{1}H NMR (300 MHz, DMSO-d6), δ (ppm): 0.96 (t, J = 7.50 Hz, 3H), 2.33 (q, J = 7.50 Hz, 2H), 3.29–3.38 (m, 4H), 3.42–3.53 (m, 4H), 4.64 (t, J = 6.00 Hz, 1H), 4.80 (t, J = 4.50 Hz, 1H).

Synthesis of *N*,*N*-bis(2-hydroxyethyl)heptanamide (mC_6). To a round bottom flask with a magnetic stir bar, diethanolamine (6.30 g, 60.0 mmol), ethyl heptanoate (4.75 g, 30.0 mmol), and sodium methoxide (0.08 g, 1.5 mmol) were added and stirred at 75 °C under vacuum for 8 h. A colorless liquid was obtained after purification of the reaction mixture using column chromatography. **mC_6**: Yield = 84.7%, ^{1}H NMR (300 MHz, DMSO-d6), δ (ppm): 0.86 (t, J = 7.50 Hz, 3H), 1.15–1.36 (m, 6H), 1.38–1.54 (m, 2H), 2.30 (t, J = 7.50 Hz, 2H), 3.29–3.38 (m, 4H), 3.41–3.52 (m, 4H), 4.65 (t, J = 4.50 Hz, 1H), 4.80 (t, J = 6.00 Hz, 1H).

Synthesis of *N*,*N*-bis(2-hydroxyethyl)palmitamide (mC_{15}). Diethanomine (6.30 g, 60.0 mmol), methyl palmitate (8.11 g, 30.0 mmol) and sodium methoxide (0.08 g, 1.5 mmol) were added to a round bottom flask equipped with magnetic stir bar. The reaction mixture was stirred at 110 °C under vacuum for 12 h. A white crystalline solid was obtained after purification using column chromatography. **mC_{15}**: Yield = 68.9%, ^{1}H NMR (300 MHz, DMSO-d6), δ (ppm): 0.85 (t, J = 7.50 Hz, 3H), 1.17–1.30 (m, 24H), 1.40–1.51 (m, 2H), 2.30 (t, J = 7.50 Hz, 2H), 3.29–3.38 (m, 4H), 3.40–3.53 (m, 4H), 4.64 (t, J = 4.50 Hz, 1H), 4.70 (t, J = 4.50 Hz, 1H).

General polyester synthesis procedure

For each polyesterification, room-temperature carbodiimide mediated polyesterification was employed as described elsewhere[15] and shown in Scheme 1. In a 500 ml round bottom flask with a magnetic stir bar, succinic acid (5.87 g, 49.6 mmol, 1.0 eq.), DPTS (5.55 g, 19.84 mmol, 0.4 eq.) and a diol monomer (**mC_2**: 8.00 g, 49.6 mmol, 1.0 eq.; **mC_6**: 10.77 g, 49.6 mmol, 1.0 eq.; **mC_{15}**: 17.02 g, 49.6 mmol, 1.0 eq.) were added along with 100 ml anhydrous CH_2Cl_2. The mixture was then cooled to 0 °C and diisopropylcarbodiimide (DIC) (23.50 mL, 148.8 mmol, 3.0 eq.) was added dropwise with a syringe. The reaction was allowed to continue over 48 hours (24 hours in case of **C_{15}**) at room temperature under N_2 atmosphere. The crude material was then subjected to vacuum filtration to remove the diisopropyl urea byproduct. The product was then concentrated under vacuum and purified *via* dialysis in MeOH (for **C_2**, and **C_6** polyesters) or by precipitation (3×) in cold MeOH (for **C_{15}** polyester). The purified polyester was further dried under vacuum to obtain the final product which was characterized with ^{1}H-NMR, GPC, DSC, rheology, and then 3D printed. **C_2**: Yield = 72.9%, ^{1}H NMR (300 MHz, $CDCl_3$), δ (ppm): 1.13 (t, J = 7.50 Hz, 3H), 2.38 (q, J = 7.00 Hz, 2H), 2.54–2.70 (m, 4H), 3.47–3.71 (m, 4H), 4.00–4.38 (m, 4H). **C_6**: Yield = 75.1%, ^{1}H NMR (300 MHz, $CDCl_3$), δ (ppm): 0.88 (t, J = 6.00 Hz, 3H), 1.15–1.43 (m, 6H), 1.60–1.63 (m, 2H), 2.34 (t, J = 7.50 Hz, 2H), 2.54–2.69 (m, 4H), 3.49–3.65 (m, 4H), 4.07–4.33 (m, 4H). **C_{15}**: Yield = 77.2%, ^{1}H NMR (300 MHz, $CDCl_3$), δ (ppm): 0.88 (t, J = 7.50 Hz, 3H), 1.18–1.34 (m, 24H), 1.55–1.56 (m, 2H), 2.34 (t, J = 7.50 Hz, 2H), 2.51–2.75 (m, 4H), 3.55–3.73 (m, 4H), 4.14–4.35 (m, 4H).

3D printing parameters

The polymers were 3D printed using a pneumatic, extrusion-based bioprinter (Cellink Inkredible+ from Cellink LLC). The polyesters were loaded into an aluminum cartridge purchased from Cellink LLC. A Teflon coated 25-gauge precision nozzle (Subrex LLC) with an inner diameter of 0.437 mm was used for all experiments. The layer height of the printed scaffolds was set to 0.3 mm (70% of nozzle inner diameter) for all experiments. The printing temperature, pressure, and speed were individually optimized for each polymer. The polyesters were printed on a glass substrate at room temperature of 23 °C. However, in case of the **C_{15}** polyester the glass substrate had to be heated to 30 °C to counteract the debonding of the scaffold from the substrate during printing. Similar issues have been reported for 3D printing of other semi-crystalline polymers like poly (lactic-*co*-glycolic acid) where the substrate temperature needs to be heated to ensure adhesion of the polymer to the substrate.[27,28] Once printed, the scaffold images were recorded using the 14MP HDMI HD Microscope USB Industrial Camera from Lapsun. The images were analyzed using ImageJ.

Results and discussion

Synthesis of monomers and polyesters

Monomer diols with 2, 6, and 15 carbons were synthesized for this study by a transamidation reaction of diethanolamine with an ethyl or methyl ester (Scheme 1). Successful synthesis

of each monomer was determined *via* ^{1}H-NMR (Fig. S1†), which can be confirmed by the appearance of the peak around 2.30 ppm for the protons on the α-carbon. This peak is a quartet for the **mC$_2$** monomer and a triplet for the **mC$_6$**, and **mC$_{15}$** monomers. The **mC$_2$** monomer had a unique triplet at 0.96 ppm for the protons on the terminal carbon of the pendant group. Both other monomers, **mC$_6$**, and **mC$_{15}$**, displayed peaks unique to the length of their side chain. The spectra for these monomers contained a multiplet around 1.46 ppm for the protons on the β-carbon, a peak around 0.85 ppm for the protons on the terminal carbon of the pendant group and a multiplet between 1.15–1.36 ppm for the protons on the carbons between the β and terminal carbons. The peaks corresponding to the two hydroxyl protons for **mC$_2$**, **mC$_6$**, and **mC$_{15}$** are all shown at 4.64 and 4.80 ppm (Fig. S1†). Overall, each *N*-substituted diol monomer was successfully synthesized.

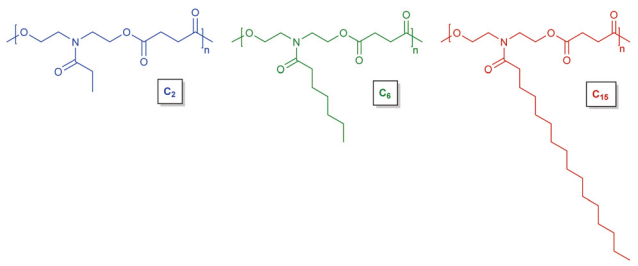

Fig. 1 Molecular structure of the C$_2$, C$_6$, and C$_{15}$ polyesters.

The synthesized polymers contain 1 : 1 molar ratio of the respective diol and succinic diacid and are labeled as **C$_2$**, **C$_6$**, and **C$_{15}$**, based on the number of carbons in the side chain (Fig. 1). The structure of the synthesized polyesters was confirmed using ^{1}H-NMR (Fig. 2). The spectra include peaks corresponding to the protons of the two carbons of succinic acid and the peaks from the individual monomers. The peaks at around 2.61 ppm correspond to the protons on the carbons of succinic acid.

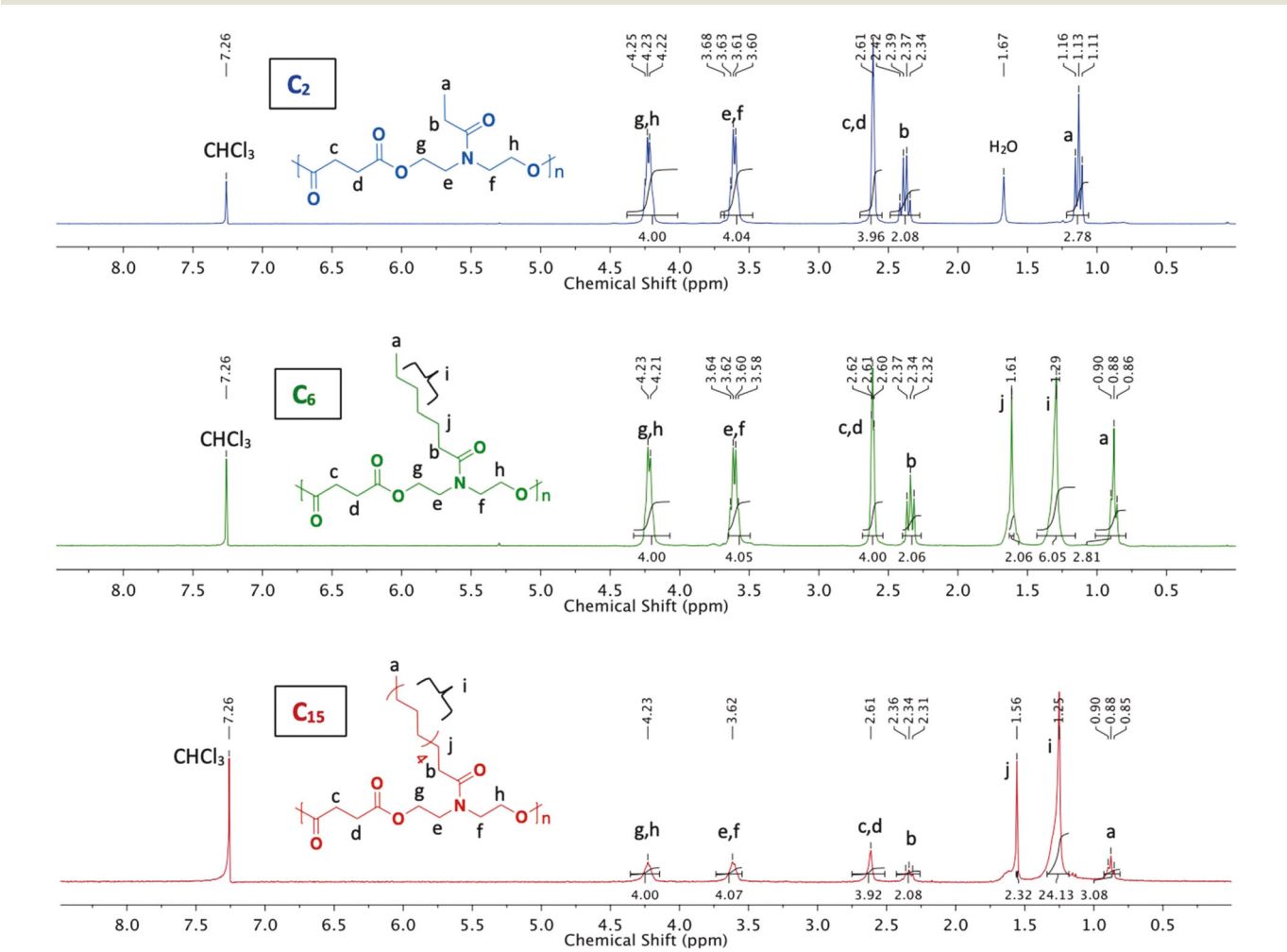

Fig. 2 Stacked ^{1}H-NMR spectra of the C$_2$ (blue), C$_6$ (green), and C$_{15}$ (red) are presented. All spectra display a singlet at 7.26 ppm corresponding to the solvent, chloroform-d.

Analysis of the polyester physical properties

The number average molecular weight (M_n) and the weight average molecular weight (M_w), glass transition temperature (T_g), melting temperature (T_m), zero-shear viscosity (η_0) and the complex modulus (G^*) of each polyester is presented in Table 1. Since the rheology of a polymer is sensitive to its molecular weight and polydispersity, polymers with similar molecular weight and polydispersity were chosen for this study.

At room temperature, the $\mathbf{C_2}$ and $\mathbf{C_6}$ polyesters are viscous whereas the $\mathbf{C_{15}}$ polyester is a brittle, white colored solid. $\mathbf{C_2}$ and $\mathbf{C_6}$ are amorphous whereas $\mathbf{C_{15}}$ is a semi-crystalline polymer. The T_g of the polymers was found to be inversely proportional to their side chain length. The T_g of the $\mathbf{C_2}$ and $\mathbf{C_6}$ polyester is 7 °C and −15 °C, respectively. $\mathbf{C_{15}}$ polyester has a T_m of about 34 °C and a re-crystallization temperature (T_c) of 23 °C (Fig. S3†), while a T_g could not be observed till −50 °C. Similar observations have been reported elsewhere.[29–31] The long unsaturated carbon side chains impede packing of the polymer backbone thereby reducing the T_g of the polymer. However, this decrease in T_g is observed only till a critical value of carbons in the side chain beyond which the side chains form ordered structures resulting in a semi-crystalline polymer.[29–31] Similarly, the long side chains of the $\mathbf{C_{15}}$ polyester form ordered structures and therefore a melting event at 34 °C can be observed. The side chain length also shows an inverse relationship with other physical properties such as viscosity and modulus. When compared at 35 °C, the $\mathbf{C_2}$ polyester has higher viscosity and modulus than the $\mathbf{C_6}$ and $\mathbf{C_{15}}$. This temperature was chosen for the rheology experiments because it is above the T_m of the $\mathbf{C_{15}}$ polyester. Due to the intrinsic nature of the technique, rheology experiments cannot be reliably performed on semi-crystalline polymers below their T_m.[32]

Rheology

The rheological behavior of a material provides insight into its 3D printability. The material should undergo shear thinning to ensure smooth, consistent extrusion of continuous filaments for extrusion-based direct-write 3D printing (EDP).[9] The viscosity of a shear thinning material reduces in response to the high shear rate at the nozzle enabling it to extrude smoothly. However, once the material is extruded the shear rate decreases dramatically and the material must be able to recover its viscosity to retain the printed shape and support overhang structures.[9] Therefore, understanding the rheology of a material as a function of shear rate can help to determine the 3D printability of the material.

The steady state viscosity as a function of shear rate at 35 °C is shown in Fig. 3A. The viscosity plateau at lower shear rates is called the zero-shear viscosity (η_0) and represents the material's viscosity at near-rest conditions.[33] The zero-shear viscosity reduces with increasing side chain lengths since the unsaturated side chains act as 'internal diluents'.[31] Therefore, the polyester with the shortest side chain ($\mathbf{C_2}$) has the highest zero-shear viscosity whereas the polyester with the longest side chain ($\mathbf{C_{15}}$) has the lowest viscosity.

The shear rate at which the drop in the viscosity begins is called the critical shear rate.[33] Here, the critical shear rate is observed to increase with increasing side chain length. The critical shear rate for the $\mathbf{C_2}$ and $\mathbf{C_6}$ polyester is 4 1 s^{-1} and 15 1 s^{-1}, respectively. Much higher shear rates are usually observed in EDP (>100 1 s^{-1}).[34] The reduction in viscosity at higher shear rates in case of the $\mathbf{C_2}$ and $\mathbf{C_6}$ polyester is indicative of the shear thinning behavior of the polymers. However, no apparent shear thinning behavior is observed for the $\mathbf{C_{15}}$ polyester for the given shear rate range. The complex viscosity (Fig. 3B) is recorded as a function of temperature by applying a small oscillatory strain. The temperature response of a polymer can be used to estimate its 3D printing temperature. The $\mathbf{C_6}$ polyester could be extruded at room temperature and therefore, it was 3D printed at 25 °C with a pressure of 250 kPa. The $\mathbf{C_2}$ polyester has similar viscosity at 50 °C as that of the $\mathbf{C_6}$ polyester at 25 °C. Therefore, the printing temperature of the $\mathbf{C_2}$ polyester was selected to be 50 °C, and the pressure was maintained at 250 kPa. The $\mathbf{C_{15}}$ polyester was printed at 35 °C which is above its T_m. However, the applied pressure was reduced to 40 kPa to compensate for the lower viscosity of $\mathbf{C_{15}}$ above its T_m.

Fig. 3C shows the steady-state viscosity of the $\mathbf{C_2}$, $\mathbf{C_6}$, and $\mathbf{C_{15}}$ polyester at their selected 3D printing temperatures of 50 °C, 25 °C, and 35 °C, respectively. The zero-shear viscosity of $\mathbf{C_2}$ and $\mathbf{C_6}$ polyester is similar, whereas the zero-shear viscosity of the $\mathbf{C_{15}}$ polyester is lower by a magnitude. The observed viscosity trend agrees with the individual 3D printing parameters of each polymer, as discussed in the next section.

Stress relaxation experiments were performed at the respective 3D printing temperatures to further understand the structure – property relationships of the synthesized polyesters. Fig. 3D shows the normalized stress relaxation modulus $G(t)$ of the polyesters in response to a step strain of 20%, which is well within the linear viscoelastic region (LVE) of each polyester. At short times, polymers show a glassy response seen as a plateau (Fig. S4†). Since $G(t)$ is a measure of elasticity, the response can be imagined as being highly elastic at first which then decays and begins to flow over large times. However, the glassy plateau region is generally not accessible using a standard melt rheometer.[33] At slightly longer times the short-range motions of the material come into play and a decrease in the relaxation modulus is observed. However, at even longer times the molecular entanglements of the polymer chains impede

Table 1 Characterization data for the $\mathbf{C_2}$, $\mathbf{C_6}$, and $\mathbf{C_{15}}$ polyesters

Polymer	M_n (kDa)	M_w/M_n	T_g (°C)	T_m (°C)	η_o [a] (kPa s)	G^* [b] (kPa)
$\mathbf{C_2}$	6.2	1.7	7.1	N/A	18.6	116.1
$\mathbf{C_6}$	8.8	1.8	−15.3	N/A	0.7	6.7
$\mathbf{C_{15}}$	8.4	1.6	N/A	34.5	0.1	0.9

[a] Zero-shear viscosity (η_o) at 35 °C. [b] Complex modulus (G^*) at 35 °C, ~10 rad s^{-1} angular frequency, and 10% strain.

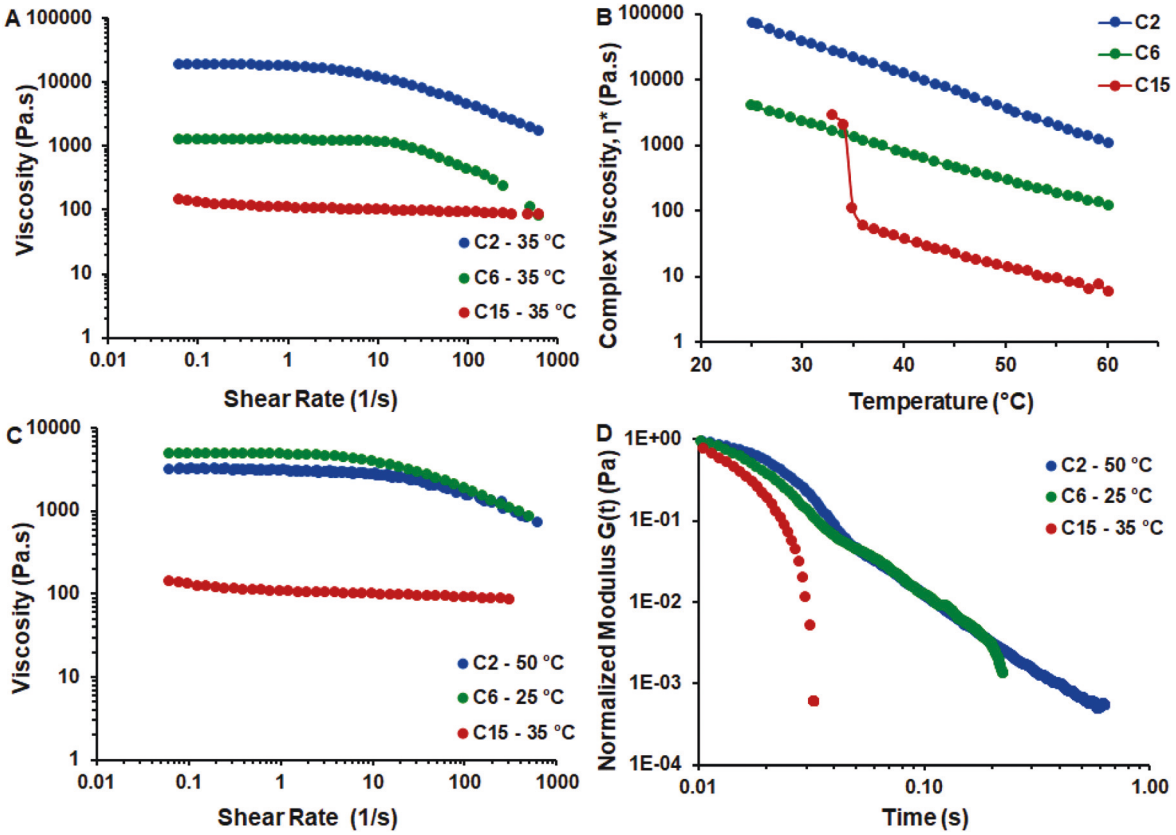

Fig. 3 (A) Steady state viscosity as a function of shear rate for the C_2, C_6, and C_{15} polyesters at 35 °C. (B) Complex viscosity as a function of temperature recorded by small amplitude oscillatory measurements. (C) Steady state viscosity as function of shear rate for the C_2, C_6, and C_{15} polyesters at their respective 3D printing temperatures. (D) Stress relaxation of the C_2, C_6, and C_{15} polyesters in response to step strain at their respective 3D printing temperatures.

the stress relaxation and a secondary plateau is observed. If the molecular weight of the polymer is below the critical entanglement molecular weight, no secondary plateau is observed, and the stress continues to fall entering the flow or terminal zone leading to total relaxation of the stress.[33] The stress relaxation plot of a general polymer is shown in Fig. S4† in the ESI.

In case of the C_2 and C_6 polyesters, a plateau-like behavior is observed at short time scales in Fig. 3D. Since the C_2 and C_6 polyesters are polydisperse, they have a range of polymer chains of different chain lengths and therefore a broad range of time scales over which the relaxation occurs resulting in the loss of a true plateau. In case of the C_{15} polyester, in addition to being polydisperse, the long side chains act as 'internal diluents' and impede inter chain entanglement leading to faster stress relaxation.[31] Overall, the C_2 and C_6 polyesters have longer relaxation times (τ_{C_2} = 83.2 ms and τ_{C_6} = 58.3 ms) than that of the C_{15} polyester ($\tau_{C_{15}}$ = 4.2 ms) (Fig. S5†). This behavior can be used to inform 3D printing parameters such as printing speed. The short relaxation times allows for printing at higher speeds.[17]

3D printing

The synthesized polyesters were 3D printed using the EDP technique where pneumatic pressure is applied to extrude continuous polymer filaments to form a 3D construct layer-by-layer. EDP is a promising 3D printing technique that allows for creating 3D objects with sizes and dimensions relevant to biomedical applications in relatively short processing times.[9] The ability to apply a range of pressures and temperatures enables printing of a wide range of materials making it one of the most versatile 3D printing techniques.[9]

The materials for extrusion-based 3D printing must meet several criteria including continuous filament extrusion, supporting overhang structures to enable porous constructs, retain the printed shape, and compatibility with the desired application like tissue engineering or drug delivery.[7] Here, we assess the 3D printability of the polymers based on their ability to satisfy the aforementioned criteria.

The first step in determining the printability of the polyesters was to ensure continuous filament extrusion. The continuous filament extrusion of a material is based on material properties such as viscosity, shear thinning, surface tension, *etc.* as well as printing conditions like temperature, pressure and nozzle length.[35] The C_6 polyester could be extruded as continuous filaments at room temperature with a pressure of 250 kPa, whereas no extrusion was observed for the C_2 and C_{15} polyester at the same conditions. The C_2 and the C_{15} polyesters

had to be heated to 50 °C and 35 °C, respectively to enable extrusion of continuous filaments (Fig. S6†). The printing pressure of 250 kPa and 40 kPa for the $\mathbf{C_2}$ and the $\mathbf{C_{15}}$ polyesters, respectively, was selected based on the mass flow rate. We hypothesize that to compare the 3D printing quality between polymers, the volumetric flow rate must be similar so that any difference in the quality of their 3D printed constructs is due to the polymer properties and not the 3D printing conditions. Since the volumetric flow rate could not be determined without dispensing a large amount of material, we calculated the mass flow rate and assume the density of the polymers to be similar.

The next step in 3D printing of the polymers is to optimize the printing speed. Ideally, the printing speed must match the extrusion flow rate so that printed filament does not stretch or sag. Therefore, 2-layer scaffolds with rectilinear infill pattern were printed at printing speeds of 30 mm min^{-1}, 45 mm min^{-1}, and 60 mm min^{-1}, while the other 3D printing parameters such as flow rate, layer thickness, nozzle diameter, matrix dimensions, and number of layers were kept the same for all polymers. The representative images of the 3D printed scaffolds are shown in Fig. 4. ImageJ was used to analyze the line width, pore area, and the printability (Pr) of the scaffolds and the analysis is shown in Fig. 5. Fig. 5A represents the line width of the 3D printed scaffolds at varying printing speeds. $\mathbf{C_6}$ and $\mathbf{C_{15}}$ have higher line widths than the $\mathbf{C_2}$ polyester at lower printing speeds. The $\mathbf{C_2}$ and $\mathbf{C_6}$ polyesters have similar viscosity at their respective printing temperatures, however, the $\mathbf{C_6}$ polyester has a much lower viscosity at room temperature and therefore its printed filament keeps deforming leading to higher line width. In case of the $\mathbf{C_{15}}$ polyester, its viscosity is lower than the $\mathbf{C_2}$ polyester which leads to higher filament deformation before the polymer re-crystallizes. The difference between the line width of the $\mathbf{C_6}$ and $\mathbf{C_{15}}$ and the $\mathbf{C_2}$ polyester is more pronounced at lower speeds where the printing times are higher and therefore the polymer filament has

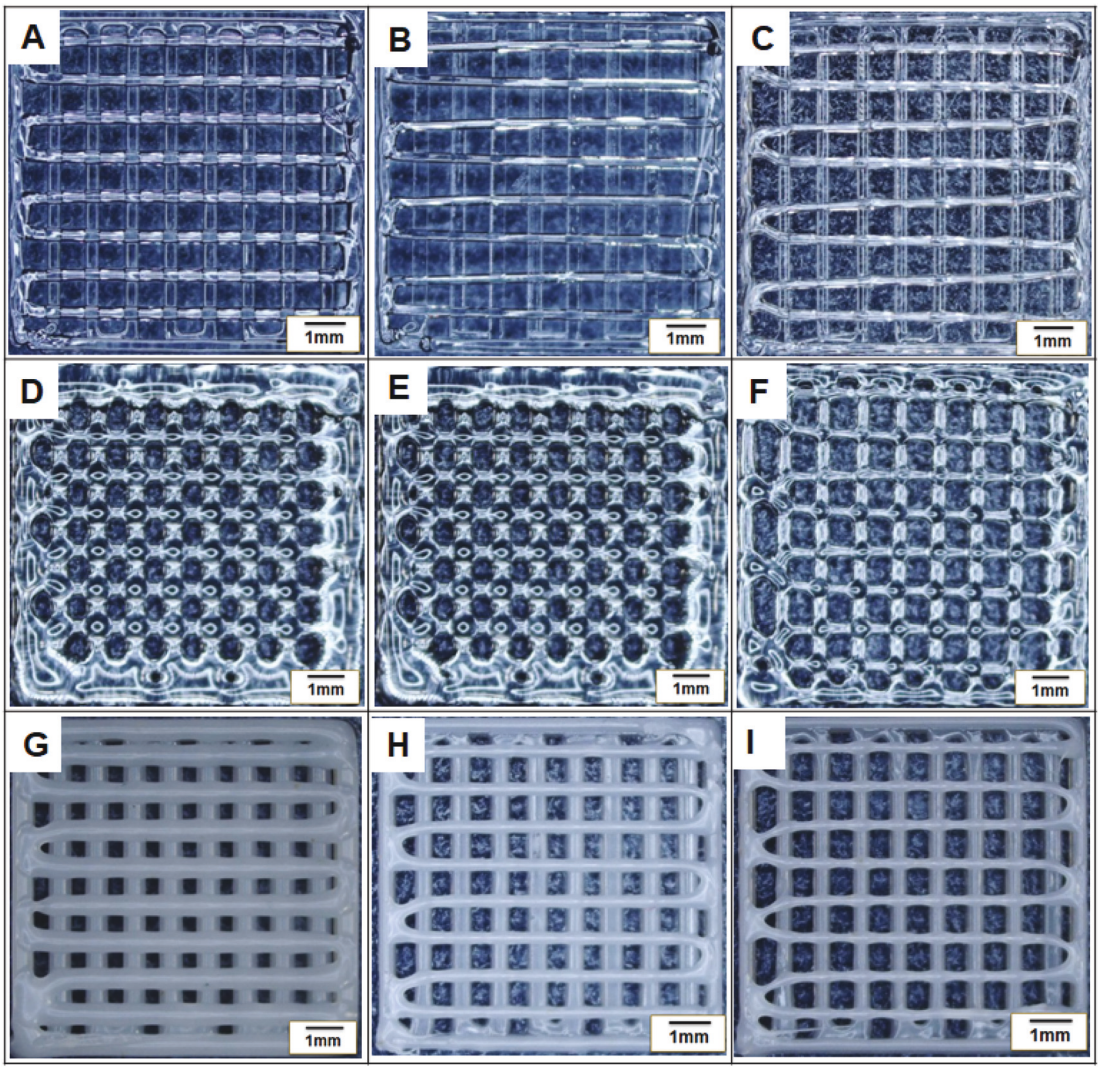

Fig. 4 2-Layered 0/90° cross-hatch patterned scaffolds of $\mathbf{C_2}$ (A–C), $\mathbf{C_6}$ (D–F), and $\mathbf{C_{15}}$ (G–I) at speed of 30 mm min^{-1}, 45 mm min^{-1}, and 60 mm min^{-1}, respectively.

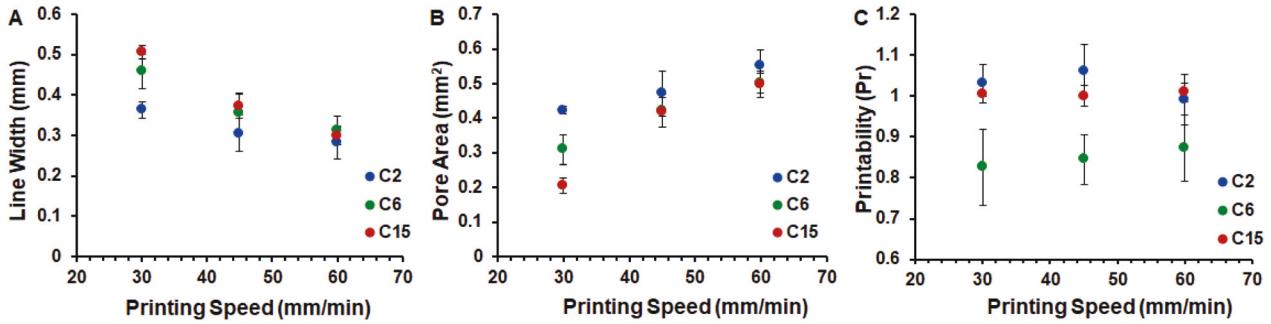

Fig. 5 (A) Line width, (B) pore area, and (C) printability of the 3D printed scaffolds of the C_2, C_6, and C_{15} polyesters.

more time to deform and spread. However, the line widths of the three polyesters approach each other at high printing speed since the time for deformation is minimum in this case. Note that the pore area has an inverse relationship with the line width and therefore the C_6 and C_{15} polyesters have relatively smaller pore area at lower speeds (Fig. 5B). The shape fidelity or printability (Pr) of the 3D printed scaffolds was measured by analyzing the shape of the pores using a shape descriptor parameter, circularity (Cr). The circularity of an enclosed area is given by Cr = 4π × (area/perimeter). Cr = 1 defines a circle. The closer the value of Cr to 1, the closer the shape is to a circle. Ideally, the shape of the pore for a 0/90° cross-hatch pattern should be square which has a Cr value of π/4. Therefore, Sun *et al.* suggested that the printability for rectilinear pattern can be defined as Pr = π/4 × (1/Cr).[36] The printability of C_2 and C_{15} polyester is close to 1 for all the printing speeds examined here. However, the printability of the C_6 polyester is closer to that of a circle (~0.78) at lower speeds (Fig. 5C) and improves slightly at higher speeds.

The C_2 polyester is printed on glass which is at room temperature, and therefore the filament cools down and retains the printed shape because of the relatively high viscosity of the polymer at room temperature (Fig. 3B). In the case of C_{15} polyester, the polyester re-crystallizes at room temperature after it is deposited and therefore retains the printed shape leading to high shape fidelity of the 3D printed construct. In contrast, the poor printability of the C_6 polyester is due to the lower viscosity of the C_6 polymer at room temperature. Once deposited onto the printing platform, the polymer keeps spreading due to the low viscosity and the two layers diffuse into each other at the intersection points leading to curved edges. Similar phenomenon has been observed for other low viscosity inks.[36] Therefore, pronounced rounded edges and poor printability values at lower speeds are observed since there is more time for the layers to diffuse.

The third step in determining material printability is to analyze the shape retention ability of the printed ink. Ideally, the 3D printed material should at least be able to retain the printed shape until it is permanently crosslinked. For most soft materials a secondary crosslinking mechanism such as ionic crosslinking, physical gelation, supramolecular interactions, or chemical crosslinking is required to permanently set the printed polymer into a 3D shape.[8,9] However, there is generally a time lag between polymer extrusion and crosslinking. In case of soft materials, the higher the time lag, greater is the deformation leading to poor shape fidelity of the 3D printed object. We compared the shape retention ability of the synthesized polyesters by monitoring the change in the scaffold pore area and printability value every 10 minutes for 1 hour. The scaffolds were printed at 30 mm min^{-1} for the C_2 polyester, and at 45 mm min^{-1} for the C_6, and C_{15} polyester. The speeds were selected to match the line width (Fig. 5A). The analysis of this deformation study is shown in Fig. 6.

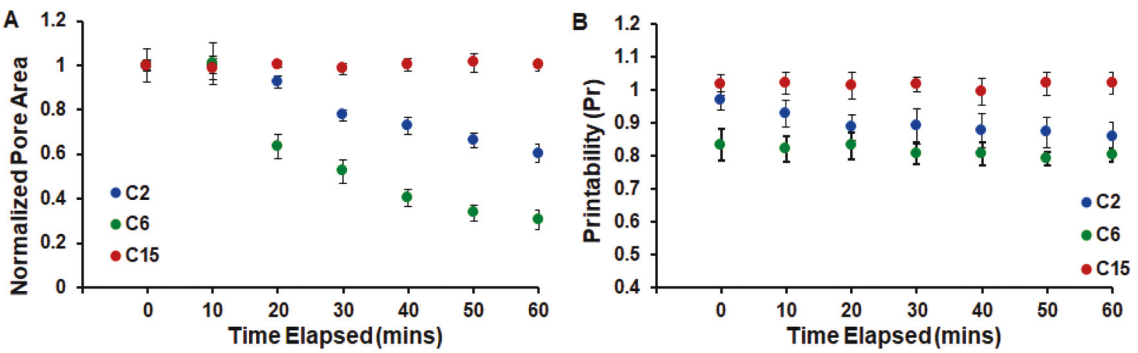

Fig. 6 (A) Normalized pore area, and (B) printability of the 3D printed scaffolds over time after 3D printing.

Fig. 6A shows the evolution of the normalized pore area with time for the 3D printed scaffolds. In case of the C_{15} polyester, the polymer re-crystallizes once deposited onto the platform and maintains the printed shape. Therefore, the pore area as well as the shape of the pore is retained as-printed for the C_{15} polyester. On the other hand, the C_2 and C_6 polyester deform continuously over time. However, the C_2 polyester deforms relatively slowly as compared to the C_6 polyester as evidenced in Fig. 6A. The pore area for the C_2 polyester decreases relatively slowly as compared to the C_6 polyester. With time the inter-layer diffusion increases, and the C_6 flows and fills some of the pores as seen in Fig. 7. The area of the filled pores was assigned a value of 0, and the average value of the total pores was used for Fig. 6A. Moreover, the shape of the pores for the C_2 polyester goes from square-like towards oval whereas for the C_6 polyesters the pore shape is already oval when the picture was taken as suggested by the printability values in Fig. 6B. The higher viscosity of C_2 polyester at room temperature slows the inter-layer diffusion. On the other hand, due to the lower viscosity of the C_6 polyester the polymer diffuses in the short time between printing of the scaffold and the first picture being taken. Other than the ability to retain the printed shape, an ideal polymer ink for EDP should be able to support free hanging filaments to create porous structures. The stability of the polyester filament was tested by printing a continuous line on top of pillars with predefined gaps of 16, 10, 7, 4, 3, 2, 1, and 0.5 mm (Fig. 8). The pictures in Fig. 8 were taken immediately after printing the line. The C_2 and C_{15} polyesters can form stable free hanging filaments spanning a distance of at least 16 mm. On the other hand, the filament sags in case of the C_6 polyester for gaps more than 7 mm and a stable filament is observed for the 4 mm and lower gap distances. The stability of the filament is a function of the elastic modulus (G') of the material.[37] The G' of C_2 poly-

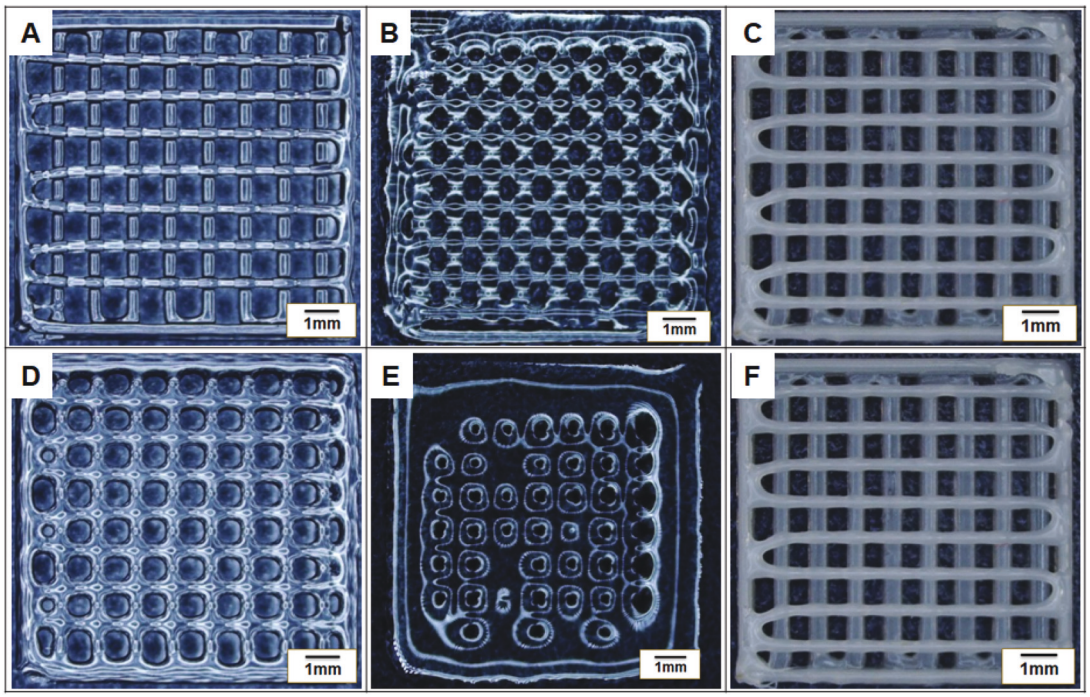

Fig. 7 Pictures of the 3D printed scaffolds of the C_2 polyester (A) at 0 min and (D) after 60 min, C_6 polyester (B) at 0 min and (E) after 60 min, and C_{15} polyester (C) at 0 min and (F) after 60 min since printing.

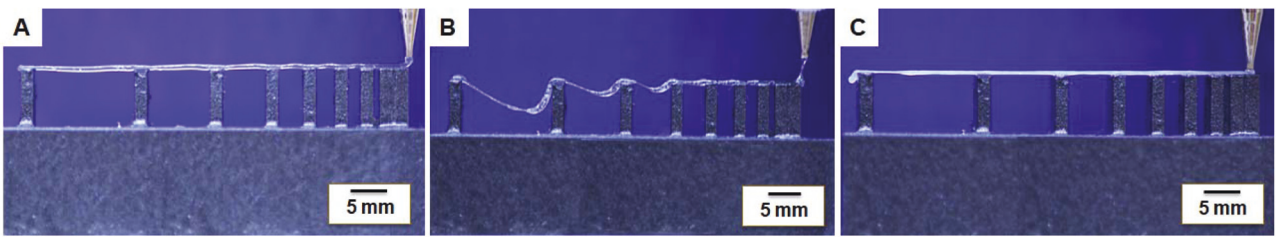

Fig. 8 Determination of maximum length of a free hanging bridge on a stage with predefined gaps (16.0, 10.0, 7.0, 4.0, 3.0, 2.0, 1.0 and 0.5 mm) of (A) C_2, (B) C_6, and (C) C_{15} polyesters.

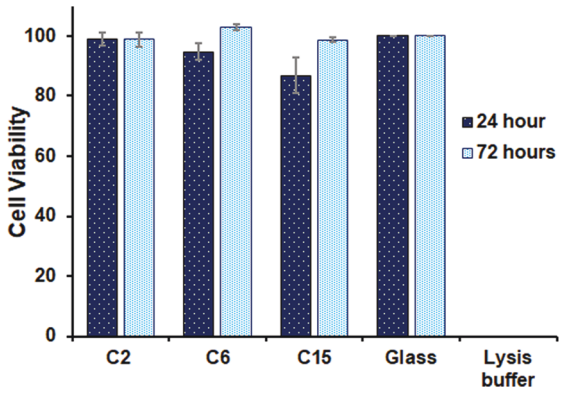

Fig. 9 % Cell viability of NIH 3T3 cells on polymer coated coverslips after 24 h and 72 h.

ester is a magnitude higher than that of $\mathbf{C_6}$ at room temperature (Fig. S6†). Although G' could not be measured for the $\mathbf{C_{15}}$ polyester at room temperature, we hypothesize that the semi-crystalline nature of the polymer imparts enough strength to sustain a free hanging filament as observed in Fig. 8C.

Cell viability

We anticipate the $\mathbf{C_2}$, $\mathbf{C_6}$, and $\mathbf{C_{15}}$ polyesters can be used for tissue engineering applications. As a preliminary assessment of cytotoxicity, we seeded NIH 3T3 mouse fibroblast cells on polymer coated coverslips. The LDH assay was used to determine viability of the fibroblasts after 24 and 72 h to show the effects of the polymer on cell viability. Glass and lysis buffer were used as positive and negative controls, respectively. As shown in Fig. 9, all three polymers exhibited minimal cytotoxicity after 24 and 72 hours of study. Furthermore, the tunability of the surface energy of the polymers (Table S2†) and the ability to add bioactive molecules and other pendant functional groups make these polymers exciting candidates for various tissue engineering applications.

Conclusions

We present the synthesis and characterization of polyesters designed for ambient temperature, additive-free, extrusion-based direct-write 3D printing. The effect of changing molecular structure of polymer on its 3D printability is also investigated. Three homo-polyesters with saturated, aliphatic side chain lengths of 2, 6, and 15 carbons were synthesized by DIC-mediated coupling and were characterized using ^{1}H-NMR, GPC and DSC. The polyesters were 3D printed using pneumatic extrusion-based direct-write technique. The 3D printability of the polyesters was assessed based on four selected criteria – continuous filament extrusion, shape fidelity, shape retention, and formation of free-hanging filaments. The 3D printing temperature and pressure was adjusted to ensure continuous filament extrusion. The shape fidelity of the polyesters was characterized based on the shape of the pores of the 3D printed, rectilinear scaffolds using a shape descriptor parameter called circularity. A printability (Pr) value was calculated based on the circularity, where Pr value of 1 represents a perfect square shaped pore. The ability of these polymers to form free hanging filaments was also compared by printing a continuous line on pillars with predefined gaps. We observed that the unsaturated carbon chains act as internal diluents and reduce the viscosity of the polyesters. The decrease in viscosity facilitates continuous extrusion of polymer filaments at low temperatures and pressures. However, beyond a critical chain length, the side chains form ordered structures leading to crystallization.

We conclude that the 3D printability of a polymer can be improved by tuning the side chain lengths. Aliphatic side chains can reduce the viscosity and enable extrusion of the polymers at low temperatures and pressures. However, the low viscosity of a polymer also diminishes its shape retention ability and the shape fidelity of the 3D printed constructs. The shape fidelity and shape retention ability can be improved by introducing supramolecular interactions in the side chains. The insights derived from this study can be used to rationally design the next generation of synthetic biomaterials that can be 3D printed at ambient temperatures and pressures without any external additives or processing aids.

Conflicts of interest

There are no conflicts to declare.

Acknowledgements

We would like to thank the National Science Foundation (DMR #1641081) for financial support.

References

1 S. V. Murphy and A. Atala, 3D Bioprinting of Tissues and Organs, *Nat. Biotechnol.*, 2014, **32**(8), 773–785.
2 D. M. Spence, C. Chen, J. L. Erkal, B. C. Gross and S. Y. Lockwood, Evaluation of 3D Printing and Its Potential Impact on Biotechnology and the Chemical Sciences, *Anal. Chem.*, 2014, **86**(7), 3240–3253.
3 C. L. Ventola, Medical Applications for 3D Printing: Current and Projected Uses, *Pharm Ther.*, 2014, **39**(10), 704–711.
4 U. Ghosh, S. Ning, Y. Wang and Y. L. Kong, Addressing Unmet Clinical Needs with 3D Printing Technologies, *Adv. Healthcare Mater.*, 2018, **1800417**, 1–24.
5 D. A. Zopf, S. J. Hollister, M. E. Nelson, R. G. Ohye and G. E. Green, Bioresorbable Airway Splint Created with a Three-Dimensional Printer, *N. Engl. J. Med.*, 2013, **368**(21), 2043–2045.
6 N. Paxton, W. Smolan, T. Böck, F. Melchels, J. Groll and T. Jungst, Proposal to Assess Printability of Bioinks for

Extrusion-Based Bioprinting and Evaluation of Rheological Properties Governing Bioprintability, *Biofabrication*, 2017, **9**(4), 044107.

7 M. Guvendiren, J. Molde, R. M. D. Soares and J. Kohn, Designing Biomaterials for 3D Printing, *ACS Biomater. Sci. Eng.*, 2016, **2**(10), 1679–1693.

8 S. C. Ligon, R. Liska, J. Stampfl, M. Gurr and R. Mülhaupt, Polymers for 3D Printing and Customized Additive Manufacturing, *Chem. Rev.*, 2017, **117**(15), 10212–10290.

9 T. Jungst, W. Smolan, K. Schacht, T. Scheibel and J. Groll, Strategies and Molecular Design Criteria for 3D Printable Hydrogels, *Chem. Rev.*, 2016, **116**(3), 1496–1539.

10 W. Khan, E. Muntimadugu, M. Jaffe and A. J. Domb, Implantable Medical Devices, in *Focal Controlled Drug Delivery*, ed. A. J. Domb and W. Khan, Springer US, Boston, MA, 2014, pp. 33–59.

11 A. Skardal and A. Atala, Biomaterials for Integration with 3-D Bioprinting, *Ann. Biomed. Eng.*, 2015, **43**(3), 730–746.

12 M. Nadgorny and A. Ameli, Functional Polymers and Nanocomposites for 3D Printing of Smart Structures and Devices, *ACS Appl. Mater. Interfaces*, 2018, **10**(21), 17489–17507.

13 T. Billiet, M. Vandenhaute, J. Schelfhout, S. Van Vlierberghe and P. Dubruel, A Review of Trends and Limitations in Hydrogel-Rapid Prototyping for Tissue Engineering, *Biomaterials*, 2012, **33**(26), 6020–6041.

14 A. E. Jakus, A. L. Rutz, S. W. Jordan, A. Kannan, S. M. Mitchell, C. Yun, K. D. Koube, S. C. Yoo, H. E. Whiteley, C. P. Richter, R. D. Galiano, W. K. Hsu, S. R. Stock, E. L. Hsu and R. N. Shah, Hyperelastic "Bone": A Highly Versatile, Growth Factor-Free, Osteoregenerative, Scalable, and Surgically Friendly Biomaterial, *Sci. Transl. Med.*, 2016, **8**(358), 1–16.

15 S. Gokhale, Y. Xu and A. Joy, A Library of Multifunctional Polyesters with "Peptide-Like" Pendant Functional Groups, *Biomacromolecules*, 2013, **14**(8), 2489–2493.

16 R. Langer and D. A. Tirrell, Designing Materials for Biology and Medicine, *Nature*, 2004, **428**(6982), 487–492.

17 S. R. Govindarajan, T. Jain, J.-W. Choi, A. Joy, I. Isayeva and K. Vorvolakos, A Hydrophilic Coumarin-Based Polyester for Ambient-Temperature Initiator-Free 3D Printing: Chemistry, Rheology and Interface Formation, *Polymer*, 2018, **152**, 9–17.

18 T. Jain, D. Saylor, C. Piard, Q. Liu, V. Patel, R. Kaushal, J.-W. Choi, J. Fisher, I. Isayeva and A. Joy, Effect of Dexamethasone on Room Temperature Three-Dimensional Printing, Rheology, and Degradation of a Low Modulus Polyester for Soft Tissue Engineering, *ACS Biomater. Sci. Eng.*, 2019, **5**(2), 846–858.

19 S. R. Govindarajan, Y. Xu, J. P. Swanson, T. Jain, Y. Lu, J. W. Choi and A. Joy, A Solvent and Initiator Free, Low-Modulus, Degradable Polyester Platform with Modular Functionality for Ambient-Temperature 3D Printing, *Macromolecules*, 2016, **49**(7), 2429–2437.

20 C. B. Highley, C. B. Rodell and J. A. Burdick, Direct 3D Printing of Shear-Thinning Hydrogels into Self-Healing Hydrogels, *Adv. Mater.*, 2015, **27**(34), 5075–5079.

21 M.-H. Huang, S. Li, D. W. Hutmacher, J.-T. Schantz, C. A. Vacanti, C. Braud and M. Vert, Degradation and Cell Culture Studies on Block Copolymers Prepared by Ring Opening Polymerization of ?-Caprolactone in the Presence of Poly(Ethylene Glycol), *J. Biomed. Mater. Res.*, 2004, **69A**(3), 417–427.

22 M. E. Hoque, W. Y. San, F. Wei, S. Li, M.-H. Huang, M. Vert and D. W. Hutmacher, Processing of Polycaprolactone and Polycaprolactone-Based Copolymers into 3D Scaffolds, and Their Cellular Responses, *Tissue Eng., Part A*, 2009, **15**(10), 3013–3024.

23 M. Zhang, A. Vora, W. Han, R. J. Wojtecki, H. Maune, A. B. A. Le, L. E. Thompson, G. M. McClelland, F. Ribet, A. C. Engler, *et al.* Dual-Responsive Hydrogels for Direct-Write 3D Printing, *Macromolecules*, 2015, **48**(18), 6482–6488.

24 D. G. Karis, R. J. Ono, M. Zhang, A. Vora, D. Storti, M. A. Ganter and A. Nelson, Cross-Linkable Multi-Stimuli Responsive Hydrogel Inks for Direct-Write 3D Printing, *Polym. Chem.*, 2017, **8**(29), 4199–4206.

25 J. S. Moore and S. I. Stupp, Room Temperature Polyesterification, *Macromolecules*, 1990, **23**(1), 65–70.

26 J. P. Swanson, M. A. Cruz, L. R. Monteleone, M. R. Martinez, P. J. Costanzo and A. Joy, The Effect of Pendant Group Structure on the Thermoresponsive Properties of N-Substituted Polyesters, *Polym. Chem.*, 2017, **8**(46), 7195–7206.

27 R. Hashemi Sanatgar, C. Campagne and V. Nierstrasz, Investigation of the Adhesion Properties of Direct 3D Printing of Polymers and Nanocomposites on Textiles: Effect of FDM Printing Process Parameters, *Appl. Surf. Sci.*, 2017, **403**, 551–563.

28 W. Z. Wu, P. Geng, J. Zhao, Y. Zhang, D. W. Rosen and H. B. Zhang, Manufacture and Thermal Deformation Analysis of Semicrystalline Polymer Polyether Ether Ketone by 3D Printing, *Mater. Res. Innovations*, 2014, **18**(suppl. 5), S5-12–S5-16.

29 S.-J. Xie, H.-J. Qian and Z.-Y. Lu, The Glass Transition of Polymers with Different Side-Chain Stiffness Confined in Free-Standing Thin Films, *J. Chem. Phys.*, 2015, **142**(7), 074902.

30 H. K. Reimschuessel, On the Glass Transition Temperature of Comblike Polymers: Effects of Side Chain Length and Backbone Chain Structure, *J. Polym. Sci., Polym. Chem. Ed.*, 1979, **17**(8), 2447–2457.

31 L. H. Sperling, *Introduction to Physical Polymer Science*, John Wiley & Sons, 2006, vol. 78.

32 M. T. Shaw, *Introduction to Polymer Rheology*, Wiley, 2012.

33 J. M. Dealy and R. G. Larson, *Structure and Rheology of Molten Polymers*, Lanser Publishers, 2006, pp. 137.

34 G. Kraut, L. Yenchesky, F. Prieto, G. E. M. Tovar and A. Southan, Influence of Shear Thinning and Material Flow on Robotic Dispensing of Poly(Ethylene Glycol) Diacrylate/Poloxamer 407 Hydrogels, *J. Appl. Polym. Sci.*, 2017, **134**(29), 45083.

35 N. Paxton, W. Smolan, T. Böck, F. Melchels, J. Groll and T. Jungst, Proposal to Assess Printability of Bioinks for Extrusion-Based Bioprinting and Evaluation of Rheological Properties Governing Bioprintability, *Biofabrication*, 2017, **9**(4), 44107.
36 L. Ouyang, R. Yao, Y. Zhao and W. Sun, Effect of Bioink Properties on Printability and Cell Viability for 3D Bioplotting of Embryonic Stem Cells, *Biofabrication*, 2016, **8**(3), 1–12.
37 J. A. Lewis, Direct Ink Writing of 3D Functional Materials, *Adv. Funct. Mater.*, 2006, **16**(17), 2193–2204.